Multipole analysis of dielectric metasurfaces composed of non-spherical nanoparticles and lattice invisibility effect

Pavel D. Terekhov,[1,2,3,4,*] Viktoriia E. Babicheva,[5] Kseniia V. Baryshnikova,[2] Alexander S. Shalin,[2] Alina Karabchevsky,[1,3,4,†] and Andrey B. Evlyukhin[2,6,7,‡]

[1] *Electrooptics and Photonics Engineering Department, Ben-Gurion University, Beer-Sheva 8410501, Israel*
[2] *ITMO University, 49 Kronversky Ave., 197101, St. Petersburg, Russia*
[3] *Ilse Katz Institute for Nanoscale Science & Technology, Ben-Gurion University, Beer-Sheva 8410501, Israel*
[4] *Center for Quantum Information Science and Technology, Ben-Gurion University, Beer-Sheva 8410501, Israel*
[5] *University of Arizona, Tucson, AZ*
[6] *Moscow Institute of Physics and Technology, 9 Institutsky Lane, Dolgoprudny 141700, Russia*
[7] *Institute of Quantum Optics, Leibniz Universitat Hannover, 30167 Hannover, Germany*

An effective semi-analytical method for analysing of the Cartesian multipole contributions in light transmission and reflection spectra of flat metasurfaces composed of identical nanoparticles is developed and demonstrated. The method combines numerical calculation of metasurface reflection and transmission coefficients with their multipole decompositions. The developed method is applied for the multipole analysis of reflection and transmission spectra of metasurfaces composed of silicon nanocubes or nanocones. In the case of nanocubes, we numerically demonstrate a "lattice invisibility effect", when light goes through the metasurface almost without amplitude and phase perturbations with the simultaneous excitation of nanoparticles multipole moments. The effect is realized due to destructive interference between the fields generated by the basic multipole moments of nanoparticles in the backward and forward directions. For metasurfaces composed of conical nanoparticles, we show that their transmission coefficient does not depend on illumination direction. In contrast, the reflection and absorption can be different for the illumination from different metasurface sides, which is associated with the excitation of different multipoles. We believe, our results could be useful for analysis and understanding of the electromagnetic properties of nanoparticle arrays and pave the way for the design of novel metasurfaces for various optical applications.

PACS numbers:

I. INTRODUCTION

High-index nanostructures and metasurfaces have been actively studied in recent years due to their promising optical properties.[1–5] Subwavelength particles with high refractive index provide the possibility to excite both electric and magnetic multipole resonances,[6–8] which can be spectrally tuned by changing the size, geometry, periodic arrangement, and surrounding conditions of the particles.[8,9] Nowadays, high-index nanostructures replace their metal counterparts for variety of applications due to high energy absorption of plasmon resonances in the optical wavelength range.[10–12] In contradiction to such plasmonic nanostructures suffering from both inter- and intraband transitions,[13] high-index materials allow light scattering without sufficient Ohmic losses. These properties of the high refractive index nanoparticles make them very attractive for practical applications in the field of optical nanoantennas,[14–18] coherent and nonlinear radiation sources,[19–22] Raman spectroscopy,[23,24] etc. The first demonstration of biosensing with silicon nanoresonators has been recently reported as well.[25] Due to scaling properties of Maxwell equations, the resonant multipole response of high-index particles can be obtained in different electromagnetic spectral ranges. For example, recently we have studied scattering properties of standalone high-refractive-index particles in the terahertz spectral range and shown the suppression of the total electric dipole moment due to the destructive interference between electric and toroidal dipole moments.[26]

The employment of high-refractive-index nanoparticles supporting electric and magnetic multipole resonances as building blocks for metamaterials (especially metasurfaces) provides new possibilities for phase-amplitude manipulations of transmitted and reflected light waves.[2–4,27] Dielectric metasurfaces appeared as a counterpart of metallic plasmonic metasurfaces in the optical range. In contrast to plasmonic structures, dielectric metasurfaces can work effectively in transmitted-light regime. Recently it has been shown that the dielectric structures can change polarization of Bessel beams and focus them.[28] In Ref.[9] it has been shown that the spectral positions of the electric and magnetic dipole resonances can be controlled by nanoparticle shape. As a result, it is possible to design dielectric (semiconductor) nanoparticles for which the electric and magnetic dipole (multipole) resonances are located at the same spectral point or overlap with each other.[17] Then it was proposed to use silicon submicron elliptical and disk particles as basic elements for the 2π variation of transmitted light phase with high transmittance efficiency.[29–31] Different realizations of dielectric metasurfaces have been suggested for the control of

light wave polarization,[32] reflection and transmission[33], e.g. using Kerker effect,[34] light color filtering[35,36] and anomalous light bending.[37] Control of a transmitted light is very important for photovoltaic applications. In Ref.[38], broadband antireflection coatings based on silicon cylinders have been suggested, and the increasing light absorption in the whole visible range has been demonstrated. Dielectric metasurfaces can be also used to control Raman scattering[39], laser[40] and light absorption[41,42] effects.

The method of the multipole decomposition of electromagnetic fields radiated by local current sources or scattered by nanoparticle structures is a powerful tool for the investigating their electromagnetic properties. There are several approaches that could be classified depending on the types of the multipoles. For example, Mie theory operates with spherical (cylindrical) multipoles being the coefficients of the field expansion in vector spherical (cylindrical) harmonics.[43] Another approach includes the Cartesian multipoles obtained with the Taylor series of the scalar Green function written in the far-field approximation.[44] Note that in this case, the Cartesian multipoles are presented in the quasi-static approximation. Recently, the Cartesian representations of the several first spherical multipoles beyond the long-wavelength approximation have been obtained and discussed.[45] In the theory of a scattering, independently on multipole representations, the multipole decomposition can provide an important information about the connection of amplitude-phase-polarization properties of a scattered radiation with the geometrical and material parameters of scatterers. Usually, this approach is applied for the investigations of optical properties of individual objects, such as nanoparticles or nanoantennas. However, the optical response of more complicated systems including metasurfaces composed of nanoparticles can be also studied using multipole decomposition.[1,33,46–49]

In this paper, we present an effective semi-analytical method for the analysis of the Cartesian multipole contributions in light transmission and reflection spectra of flat metasurfaces composed of identical nanoparticles. Generally, the method includes the following stages: i) the numerical calculation of the total electromagnetic fields inside metasurface building blocks, and the transmission and reflection coefficients; ii) the calculation of nanoparticles' multipole moments using the total electromagnetic fields; iii) the multipole decompositions of the reflection and transmission coefficients. Note that analytical studies of nanoparticles and their arrays are possible in a very limited number of cases and basically it is concerned only the spherical nanoparticles and infinitely-long cylindrical nanorods.[43] In the case of arbitrarily-shaped nanoparticles, a full-wave numerical simulation of the structure composed of the nanoparticles is critical for studying their optical properties. Multipole decomposition of electromagnetic fields presented in this article is built upon the full-wave numerical simulations and is essentially the next step in the analysis of metasurfaces. Using numerical simulations, we make sure that all structure features, such as particles shape and inter-particle coupling, are correctly taken into account; and further, using analytical expressions for each multipole, we analyze their role and contribution to observed optical effects. Thus, we believe that a full-wave numerical simulation together with the multipole decompositions is a powerful tool and significantly broadens a range of problems that can be investigated.

Generally speaking, for the calculations of separate multipole contributions to a scattered electric field, which determines the transmission and reflection coefficients of an array, it is important to know the field propagators for each multipole moment. For the dipole sources, the analytical expressions of the propagators are well known and presented in Ref.[1] for the periodic metasurfaces. However, for the higher order multipoles, such as quadrupoles and octupoles, the analytical descriptions are not trivial. Here we demonstrate a straightforward method allowing to obtain the multipole decomposition of the transmission and reflection coefficients of metasurfaces up to electric octupole taking into account interactions between the meta-atoms.

In our work, we consider systems in the framework of the classical approach that is used for the description of electromagnetic fields and particle's responses. In the framework of semi-classical formalism, when only electromagnetic fields are considered as classical, our multipole method could be applied to the systems similar to that of Ref.[50], where arrays composed of atoms have been studied in the dipole approximation. However, the multipole moments of atoms need to be calculated using a quantum approach.

In the next sections, we explain how the multipole decompositions for a metasurface can be obtained, then we apply the developed approach for the analysis of the transmission and reflection spectra of the metasurfaces composed of cubic and conical silicon nanoparticles. We reveal and explain in details the strong suppression of the reflection from the metasurfaces, taking place due to the generalized Kerker effect and so-called invisibility effect (anapole-like behavior).[51–53] In the latter case, light waves transmit metusrfaces almost without amplitude and phase changes.

II. MULTIPOLE REPRESENTATION OF REFLECTION AND TRANSMISSION COEFFICIENTS

In order to develop multipole representations of the transmission and reflection coefficients, we use the results from the paper[1], where reflection and transmission properties of silicon spherical nanoparticle arrays are theoretically investigated in the point electric- and magnetic-dipole approximation. It has been demonstrated that for the normal light incidence with the linear polarization along x-axis (as shown in Fig. 1) the electric field reflection r and transmission t coefficients of rectangular 2D

infinite arrays of identical spherical nanoparticles can be written as

$$r = \frac{ik_d}{2S_L}\left[\alpha^E_{eff} - \alpha^M_{eff}\right], \tag{1}$$

$$t = 1 + \frac{ik_d}{2S_L}\left[\alpha^E_{eff} + \alpha^M_{eff}\right], \tag{2}$$

where $k_d = k_0\sqrt{\varepsilon_d}$ is the wavenumber in a surrounding medium (k_0 is the wavenumber in vacuum), S_L is the area of a lattice unit cell ($S_L = D^2$ for the square lattice, where D is the lattice constant), ε_0 is the vacuum permittivity, and ε_d is the permittivity of a surrounding medium. The effective electric α^E_{eff} and magnetic α^M_{eff} dipole polarizabilities are determined by the expressions

$$\alpha^E_{eff} = \frac{1}{\varepsilon_0\varepsilon_d/\alpha^E - k_d^2 G^0_{xx}}, \tag{3}$$

$$\alpha^M_{eff} = \frac{1}{1/\alpha^M - k_d^2 G^0_{yy}}, \tag{4}$$

where α^E and α^M are electric and magnetic polarizabilities of single particles, respectively, and G^0_{xx} and G^0_{yy} are the dipole sums taking into account the influence of electromagnetic coupling between the nanoparticles in the array on their dipole moments.[33] In our case, only p_x-component of electric and m_y-component of magnetic dipole moments are not equal to zero and can be written as

$$p_x = \varepsilon_0\varepsilon_d\alpha^E_{eff}E_0, \qquad m_y = \alpha^M_{eff}H_0, \tag{5}$$

where E_0 and H_0 are electric and magnetic fields of the normally incident plane waves at the points of dipole locations, $H_0 = (\varepsilon_0\varepsilon_d/\mu_0)^{1/2}E_0$ (where μ_0 is the vacuum magnetic permeability). Note that all the nanoparticles of the infinite array have the same electric and magnetic dipole moments because of nanoparticle equality and the normal incidence of light waves. Replacing the effective polarizabilities in (1) and (2) by the corresponding dipole moments one can obtain

$$r = \frac{ik_d}{E_0 2S_L\varepsilon_0\varepsilon_d}\left[p_x - \frac{1}{v_d}m_y\right], \tag{6}$$

$$t = 1 + \frac{ik_d}{E_0 2S_L\varepsilon_0\varepsilon_d}\left[p_x + \frac{1}{v_d}m_y\right], \tag{7}$$

where $v_d = 1/\sqrt{\mu_0\varepsilon_0\varepsilon_d}$ is the speed of light in the surrounding nonmagnetic medium. These equations (6) and (7) are the representation of the reflection and transmission coefficients in the dipole moment approximation.

In order to estimate the contributions of high-oder multipole moments (up to the third order) in the reflection and transmission coefficients, let us consider the multipole representation of the scattered electric field $\mathbf{E}^{\rm sc}_0$ obtained for a single nanoparticle[54–57]

$$\begin{aligned}\mathbf{E}^{\rm sc}(\mathbf{n}) \;\sim\; & \Big([\mathbf{n}\times[\mathbf{p}\times\mathbf{n}]] + \frac{1}{v_d}[\mathbf{m}\times\mathbf{n}] \\ & + \frac{ik_d}{6}[\mathbf{n}\times[\mathbf{n}\times\hat{Q}\mathbf{n}]] + \frac{ik_d}{2v_d}[\mathbf{n}\times(\hat{M}\mathbf{n})] \\ & + \frac{k_d^2}{6}[\mathbf{n}\times[\mathbf{n}\times\hat{O}(\mathbf{nn})]]\Big),\end{aligned} \tag{8}$$

where $\mathbf{n}$ is the unit vector indicating the scattering direction, $\mathbf{p}$ and $\mathbf{m}$ are the total electric (TED) and magnetic dipole (MD) moments, $\hat{Q}$, $\hat{M}$ and $\hat{O}$ are the symmetrized and traceless tensors of electric quadrupole (EQ), magnetic quadrupole (MQ) and electric octupole (EOC) moments, respectively. The expressions in the brackets in (6) and (7) can be obtained from (8) if we consider the dipole terms only and take into account only the forward scattering for transmission and the backward scattering for reflection. For the forward scattering $\mathbf{n} = (0,0,1)$, and the backward scattering $\mathbf{n} = (0,0,-1)$. Inserting $\mathbf{n} = (0,0,n_z)$ in (8) we obtain

$$\begin{aligned}E^{\rm sc}_x \;\sim\; & \Big(p_x n_z^2 + \frac{1}{v_d}m_y n_z - \frac{ik_d}{6}Q_{xz}n_z^3 \\ & - \frac{ik_d}{2v_d}M_{yz}n_z^2 - \frac{k_d^2}{6}O_{xzz}n_z^4\Big),\end{aligned} \tag{9}$$

$$\begin{aligned}E^{\rm sc}_y \;\sim\; & \Big(p_y n_z^2 - \frac{1}{v_d}m_x n_z - \frac{ik_d}{6}Q_{yz}n_z^3 \\ & + \frac{ik_d}{2v_d}M_{xz}n_z^2 - \frac{k_d^2}{6}O_{yzz}n_z^4\Big).\end{aligned} \tag{10}$$

In the dipole approximation, the scattering amplitudes (9) and (10) are

$$E^{\rm sc}_x \;\sim\; \left(p_x \mp \frac{1}{v_d}m_y\right), \tag{11}$$

$$E^{\rm sc}_y \;\sim\; \left(p_y \pm \frac{1}{v_d}m_x\right), \tag{12}$$

where the upper (lower) sign corresponds to the backward (forward) scattering. Comparing (11) with the expressions for the reflection and transmission coefficients (6) and (7), we get the straightforward conclusion: the multipole representation of the reflection and transmission coefficients can be obtained by the replacing of the expressions in the brackets of (6) and (7) by the multipole decompositions of the single particle scattering amplitude (9) or (10) depending on the polarization of the

incident waves. Finally, in the case of the x-polarization

$$r = \frac{ik_d}{E_0 2S_L\varepsilon_0\varepsilon_d}\left(p_x - \frac{1}{v_d}m_y + \frac{ik_d}{6}Q_{xz} - \frac{ik_d}{2v_d}M_{yz} - \frac{k_d^2}{6}O_{xzz}\right), \quad (13)$$

$$t = 1 + \frac{ik_d}{E_0 2S_L\varepsilon_0\varepsilon_d}\left(p_x + \frac{1}{v_d}m_y - \frac{ik_d}{6}Q_{xz} - \frac{ik_d}{2v_d}M_{yz} - \frac{k_d^2}{6}O_{xzz}\right), \quad (14)$$

in the case of the y-polarization

$$r = \frac{ik_d}{E_0 2S_L\varepsilon_0\varepsilon_d}\left(p_y + \frac{1}{v_d}m_x + \frac{ik_d}{6}Q_{yz} + \frac{ik_d}{2v_d}M_{xz} - \frac{k_d^2}{6}O_{yzz}\right), \quad (15)$$

$$t = 1 + \frac{ik_d}{E_0 2S_L\varepsilon_0\varepsilon_d}\left(p_y - \frac{1}{v_d}m_x - \frac{ik_d}{6}Q_{yz} + \frac{ik_d}{2v_d}M_{xz} - \frac{k_d^2}{6}O_{yzz}\right). \quad (16)$$

The reflection and transmission coefficients are

$$R = |r|^2, \qquad T = |t|^2. \quad (17)$$

Then the absorption coefficient A could be derived from the following expression $A = 1 - R - T$.

In next section, we numerically prove that the multipole expressions for T and R obtained above are in excellent agreement with the direct numerical calculations of the transmission and reflection for periodic dielectric metasurfaces.

III. MULTIPOLE ANALYSIS OF SILICON METASURFACES

In this section, we implement our method to analyse optical properties of silicon metasurfaces in air, and reveal some special effects. As examples we consider two types of metasurfaces composed of cubic or conical nanoparticles. Here, total electric fields in nanoparticles, composing metasurfaces, and corresponding reflection and transmission spectra are calculated numerically using finite element method in COMSOL Multiphysics; the Cartesian multipole moments of the nanoparticles are calculated following their definitions presented in Ref.[45] with replacement of the current density by the induced polarization $\mathbf{P}$ (see Appendix); the multipole contribution in the reflection and transmission coefficient are estimated on the basis of the above equations. Note that, at the condition of normal incidence of linear polarized light waves on a flat infinite metasurface composed of identical nanopaticles, the every nanoparticle will have the same electric and magnetic multipole moments calculated with respect of its center of mass. In this article we consider that infinite metasurfaces are placed in a homogeneous surrounding medium with $\varepsilon_d = 1$.

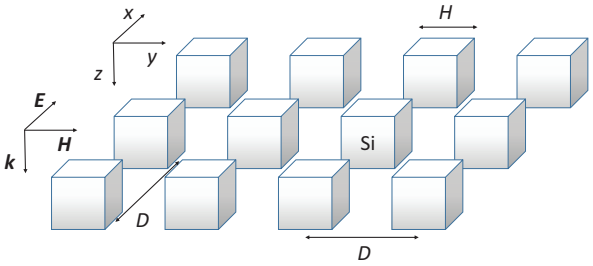

Figure 1: Artistic representation of the considered silicon metasurface composed of nanocubes (infinite nanostructure illuminated with the linearly polarized plane wave).

A. Metasurfaces composed of silicon nanocubes

1. *Multipole decomposition*

Let us apply our approach to analyse the optical properties of the metasurfaces depicted in Fig. 1 and normally irradiated by a linear E_x-polarized plane wave. The nanoparticles with size $H = 250$ nm are considered. The spectra of transmission, reflection, and absorption coefficients and the corresponding mutipole decompositions are presented in Fig. 2 for two metasurfaces with a different periodicity. The reflection and transmission spectra numerically calculated are in excellent agreement with the corresponding spectra calculated with (13), (14), and (17) (Fig. 2 a,c). The spectral features (maxima and minima) observed in Fig. 2a and Fig. 2c can be analyzed using the multipole decompositions presented in Fig. 2b and Fig. 2d, respectively.

Now let us demonstrate the influence of the electromagnetic interactions between nanoparticles in the arrays on their multipole response. In Fig. 2b,d we show the absolute values of the multipole contributions in r and t coefficients of two metasurface with different periods. Similar values of the multipole contributions in scattered electric-field amplitude (Eq. 9) for an individual nanocube placed in free space are given in Fig. 2e. The comparison between Fig. 2b and Fig. 2e shows that the resonances of the electric and magnetic quadrupole moments in the array structure with the large period ($T = 400$ nm) are realized in the same spectral region with a small blue shift of EQ peak. However, the behavior of the total electric dipole moment and the magnetic dipole moment differs. In the case of the periodic structure with $T = 400$ nm, smooth TED resonance of the single particle acquires a pronounced peak in the region around $\lambda = 840$ nm (Fig. 2b). Moreover, MD resonance

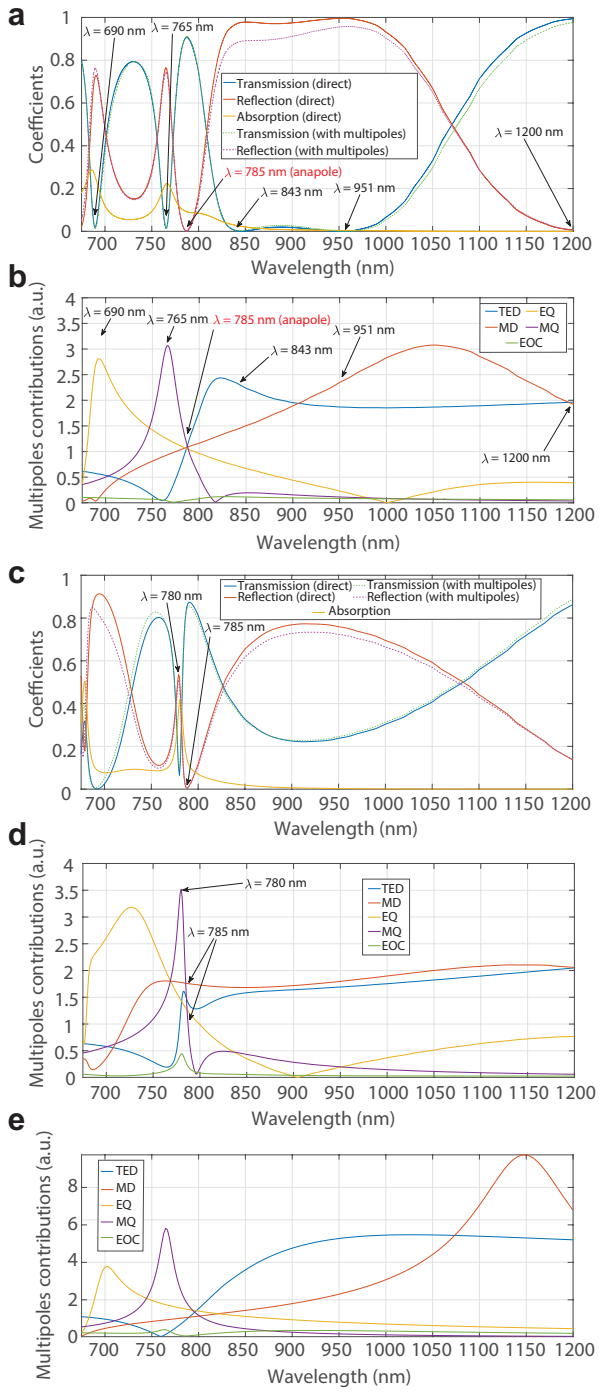

Figure 2: Spectra of the transmission T, reflection R, and absorption A coefficients of the metasurfaces composed of silicon nanocubes of height $H = 250$ nm with period (a) $D = 400$ nm and (c) $D = 300$ nm. (b),(d) Absolute values of the multipole contributions in the electric field reflection and transmission coefficients r and t: panel (b) corresponds to $D = 400$ nm (same as (a)) and panel (d) corresponds to $D = 300$ nm (same as (b)). (e) Absolute values of the multipole contributions in the scattered electric-field amplitude (see. Eq. (8)) calculated for a single silicon nanocube with size $H = 250$ nm in air.

becomes much broader and shifts to the blue side due to the electromagnetic interaction between nanocudes (Fig. 2b). Interestingly, the absolute values of all multipole contributions are approximately equal to each other near the wavelength of $\lambda = 785$ nm in the both cases presented in Fig. 2b and Fig. 2e. For a single particle, the similar combination leads to the side-scattering effect.[17] In the case of arrays, this could provide conditions for the so-called "lattice anapole (invisibility) effect" (see below). Note that the zero contributions of EQ ($\lambda = 1000$ nm), MQ ($\lambda = 820$ nm), and MD ($\lambda = 690$ nm) in Fig. 2b are results of the multipole coupling in array structures.

Decrease of the array period provides stronger electromagnetic inter-particle interaction that in turn results in the more pronounced changes of the spectral distribution of the multipole resonances in the arrays in comparison with the case of the single nanoparticles (compare the multipole decompositions shown in Fig. 2e and in Fig. 2d). In the latter case, the multipole contributions are calculated for the array with the period of $D = 300$ nm. One can see from Fig. 2d that there is the resonant TED-MQ-EOC coupling around $\lambda \approx 780$ nm, where the three resonant peaks of TED, MQ, and EOC appear (Fig. 2d). This coupling provide the resonant peak of the absorption coefficient in the area of MQ resonance (Fig. 2c).

2. *Multipole analysis implementation*

Let us consider in details the optical properties of the metasurfaces with $D = 400$ nm. In Fig. 2a,b, different minima and maxima are marked by black arrows, and these spectral features in the transmission and reflection coefficients are analyzed with help of the multipole decomposition approach. For this purpose we consider both the magnitudes (Fig. 2b) and phases (Fig. 3a) of multipole contributions in (13) and (14). It is convenient to use the following presentations for the electric field reflection (13) and transmission (14) coefficients:

$$r = i|C|(A_p e^{i\varphi_p} - A_m e^{i\varphi_m} + A_Q e^{i\varphi_Q} - A_M e^{i\varphi_M} - A_O e^{i\varphi_O}), \quad (18)$$

$$t = 1 + i|C|(A_p e^{i\varphi_p} + A_m e^{i\varphi_m} - A_Q e^{i\varphi_Q} - A_M e^{i\varphi_M} - A_O e^{i\varphi_O}), \quad (19)$$

where A_p, A_m, A_Q, A_M, A_O are the absolute values (magnitudes) of the ED, MD, EQ, MQ, and EOC terms, respectively (shown in Fig. 2b) from the electric field reflection r and transmission t coefficients , and:

$$C = \frac{k_d}{E_0 2 S_L \varepsilon_0 \varepsilon_d}, \quad (20)$$

φ_p, φ_m, φ_Q, φ_M, and φ_O are the phases of the ED, MD, EQ, MQ, and EOC terms, respectively, with the inclusion of the phase corresponding to the factor C. Note that the phase of the factor C originates from the incident electric

field E_0. In our case the spectrum of the E_0 phase is shown in Fig. 4 (the green line). The plots of the phases from (18) and (19) are presented in Fig. 3a. Note that the EOC contribution in the reflection and transmission (Fig. 2b) is very small for the whole considered spectral range, and, hereinafter, it will not be taken into account in the multipole analysis.

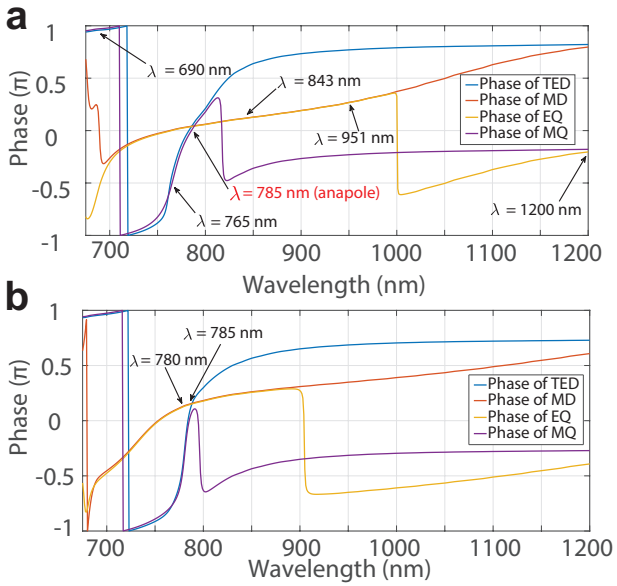

Figure 3: Phases of the multipole terms in the amplitude reflection and transmission coefficients of the metasurface composed of nanocubes for (a) $D = 400$ nm and (b) $D = 300$ nm. Definition of the phase is explained in the main text.

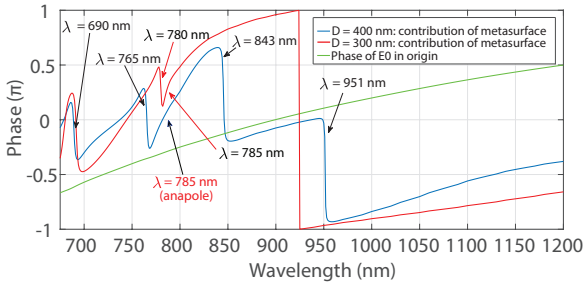

Figure 4: Phases of the electric field in the system of periodic nanocubes: the blue and red lines are for the phase difference between the incident wave and the transmitted wave for D = 400 and 300 nm correspondingly; the green line is for the phase of the electric field in the plane of the point-multipoles positions.

Let us analyze the transmission minima and maxima comparing the data presented in Fig.2a and Fig.2b. Pronounced transmission dip at the wavelength $\lambda = 690$ nm (Fig. 2a) mainly corresponds to the EQ resonance (Fig. 2b). In general, MQ and TED contributions should also be taken into account in this wavelength range (Fig. 2b). So, the approximation of (18) and (19) for this wavelength gives

$$r \approx i|C|(-A_p - iA_Q + A_M) \approx |C|A_Q, \qquad (21)$$

$$t = 1 + i|C|(-A_p + iA_Q + A_M) \approx 1 - |C|A_Q, \qquad (22)$$

where we use that $\varphi_p = \varphi_M \approx \pi$, $\varphi_Q \approx -\pi/2$ (Fig. 3a for $\lambda = 690$ nm), and $A_p \approx A_M$ (Fig. 2b also for $\lambda = 690$ nm). Thus, the multipole analysis shows that this suppression of the transmission is solely determined by the EQ resonance.

The next case that deserves attention is the transmission dip at wavelength $\lambda = 765$ nm (Fig 2a). This effect is determined basically by the MQ resonance. Noticeable separate contributions of MD and EQ multipoles (Fig 2b) compensate each other because of their phases. Indeed, from Fig. 3a for $\lambda = 765$ nm one can see that $\varphi_m = \varphi_Q = 0$ and $\varphi_M = -\pi/2$. Moreover, $A_m \approx A_Q$ (Fig. 2b). Thus, using (18) and (19) we get $r \sim A_M$ and $t \approx 1 - |C|A_M$.

The broad spectral band of the transmission suppression between $\lambda = 843$ nm and $\lambda = 951$ nm in Fig. 2a is realized due to the strong TED and MD scattering in the forward and backward directions. The destructive interference between the incident wave and the strong forward scattering provides the transmission suppression.

The significant reflection suppression at $\lambda = 1200$ nm (Fig. 2a) takes place because of the realization of the Kerker effect[34] in periodic array structures. At these conditions, array's optical response is provided basically by the TED and MD contributions for which the relations $A_p = A_m$ and $\varphi_p = \varphi_m$ are fulfilled.

3. *Lattice invisibility*

Let us now pay a particular attention to the important and unusual effect at $\lambda \approx 785$ nm, where the reflection is totally suppressed (Fig 2a) and the absolute values of the multipole (TED, MD, EQ, and MQ) contributions to r, t coefficients are nearly equal to each other, so that $A_p = A_m = A_Q = A_M$ (Fig 2b, $\lambda \approx 785$ nm). Moreover, the phases of these multipole contributions are also very close to each other and equal to zero approximately (Fig. 3a, $\lambda \approx 785$ nm). In this case, we obtain from (18) and (19) for the field reflection and transmission coefficients

$$r \approx i|C|(A_p - A_m + A_Q - A_M) = 0, \qquad (23)$$

$$t \approx 1 + i|C|(A_p + A_m - A_Q - A_M) = 1. \qquad (24)$$

It means that the light passes through the metasurface without perturbations. From the Fig. 4 (blue line) one can see that the metasurface contribution to the transmitted wave phase is also zero, so it is equal to the phase of the incident wave at $\lambda \approx 785$ nm. In its turn, this unusual behaviour of the light looks like to the case of

the absent metasurface or the metasurface, which doesn't interact with the light. The multipole analysis following from (23) and (24) provides important information about the origin of this effect. The reflection suppression could be considered as a realization of the generalized Kerker effect,[47] namely: the suppression of the backward scattering is provided by the destructive interference between the waves scattered by the TED and MD moments and by the destructive interference between the waves scattered by the EQ and MQ moments. However, here is also the simultaneous suppression of the scattering in the forward direction that does not belong to the effects of Kerker's type. In the case of the forward scattering the TED and MD moments generate (scatter) the waves in phase with respect to each other. Moreover, the MQ and EQ moments also generate (scatter) the waves in phase with respect to each other. Therefore, the suppression of the forward scattering is realized only due to the destructive interference between the waves separately generated (scattered) by the dipole-type and quadrupole-type multipoles. In the case of a single nanocube the similar relation between multipoles leads to the isotropic side scattering.[17] The light transmission through a resonant system without perturbation of both amplitude and phase could be referred to a *lattice invisibility effect* or as extraordinary transmission photonic effect. It means that an electromagnetic energy is accumulated in scatterers but the total electromagnetic fields outside the scatterers mimic the incident fields almost without distortion as it can be seen from Fig. 5a. We call such behavior "lattice anapole effect" because this effect is similar to the light scattering by the particles in anapole states,[51] when the particles do not scatter providing the non-perturbed incident wave. From the physical point of view, however, there are always weak contributions of the non-resonant high order multipoles that affect the transmission amplitude and phase. For example, for the case considered here it concerns the contribution of EOC moment shown in Fig 2b for $\lambda = 785$ nm. These weak contributions provide satisfaction of the optical theorem[54] in the scattering.

4. *Denser metasurfaces*

Concluding this subsection we consider the metasurface where the distance between the nanocubes is smaller than discussed above. Transmission, reflection, and absorption spectra of the metasurface with $D = 300$ nm are shown in Fig. 2c. The absolute values of the multipole contributions for this case are presented in Fig. 2d. Note that there are no spectral points, where the contributions of the mutipoles coincide. However, one can see from Fig. 2c that there is a reflection suppression band around $\lambda = 785$ nm. The application of the multipole analysis for the point $\lambda = 785$ nm gives the following relations: $A_M < A_Q < A_p < A_m$ (Fig. 2d) and $\varphi_M < \varphi_Q \approx \varphi_p \approx \varphi_m$ (Fig. 3b). This means that

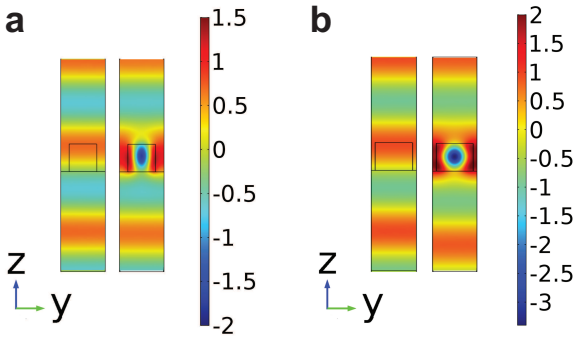

Figure 5: Fragment of the spatial electric field distribution in the zy-plane at $\lambda = 785$ nm for (a) $D = 400$, (left) only incident field, (right) total electric field; (b) $D = 300$ nm, (left) only incident field, (right) total electric field. The black contours indicate the position of a nanocube in the metasurfaces

the effect of the *unperturbed* transmission corresponding to the expressions (23) and (24) is not realized in the metasurface at this wavelength, and the phase of transmitted light differs from the phase of the incident wave (Fig. 5b).

B. Metasurface composed of silicon nanocones

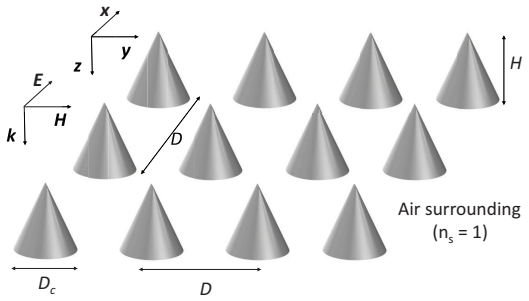

Figure 6: The artistic representation of the considered silicon metasurface based on nanocones (infinite nanostructure illuminated by a linearly E_x-polarized plane wave).

The next example considered here is the metasurface composed of the silicon nanocones of height $H = 300$ nm and base diameter $D_c = 300$ nm. A fragment of the metasurface is schematically presented in Fig. 6. The main difference between the cases of cubical and conical particles is in their symmetrical properties; while cubes are symmetric with respect to the incidence direction (upward or downward), cones are not. We describe and compare transmission, reflection, and absorption spectra and corresponding multipole contributions to the amplitude reflection and transmission coefficients for the two aforementioned irradiation regimes (Fig. 7). From Fig. 7a,c

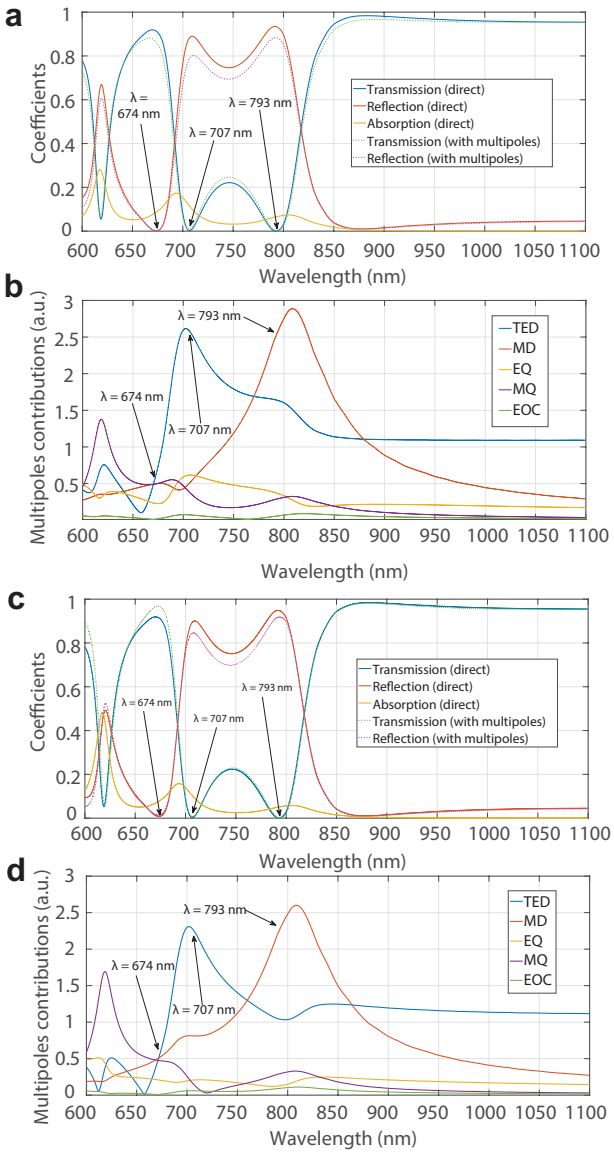

Figure 7: Spectra of the transmission T, reflection R, and absorption A coefficients of the metasurface composed of the silicon nanocones with $H = 300$ nm, $D_c = 300$ nm with period $D = 450$ nm for (a) illumination from top of the nanocones (c) illumination from the base side. (b,d) Absolute values of the multipole contributions in the amplitude coefficients r and t: panel (b) corresponds to the illumination from top of the nanocones (same as (a)), and panel (d) corresponds to illumination from base edge of the nanocones (same as (b)).

it is clearly seen that the suggested multipole decomposition (17) correctly corresponds to the numerical calculations of the transmission and reflection for both cases of irradiation (some discrepancy in the short wavelengths regions is associated with the influence of the higher order multipoles). Due to the fact that the extinction does not depend on the irradiation direction, the numerically calculated transmission spectra presented in Fig. 7a,c are unchanged with the variation of the illumination condi-

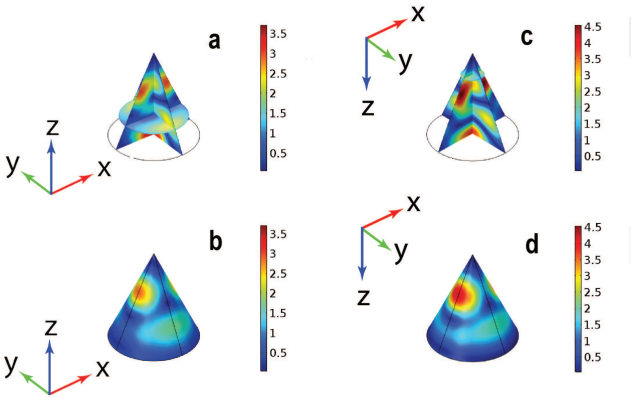

Figure 8: Electric field distribution inside and on the surface of one conical nanoparticle from the considered silicon metasurface ($H = 300$ nm, $D = 450$ nm) at the wavelength $\lambda = 619$ nm for the illumination (a,b) from top of the cones (c,d) from the base.

tions. However, the reflection and absorption coefficients can change their spectral properties. This effect could be associated with the changes of the total electric and magnetic field distributions inside the nanocones irradiated in the opposite directions (see, for example, Fig. 8). As a result, one can see some differences between the multipole contributions presented in Fig. 7b and Fig. 7d.

For the application of the multipole analysis several spectral points at wavelengths $\lambda = 619$, 674, 707, and 794 nm are selected in Fig. 7. The narrow transmission minimum at the wavelength $\lambda = 619$ nm basically corresponds to the resonant excitation of MQ moment for both illumination directions. However, the contributions of other multipoles are different for the different illumination conditions (compare Fig. 7b and Fig. 7c near $\lambda = 619$ nm), because in this case we have different distributions of the electric field inside the nanoparticles and shown in Fig. 8.

Importantly, in contrast to the case of nanocubes, there are no spectral points where the values of the multipole contributions are equal to each other in terms of both phase and amplitude (Fig. 7b,d). The lack of such points means that lattice invisibility is not realized in this metasurface. At the wavelength $\lambda = 674$ nm there is a strong suppression of the reflection (Fig.7a,c). For this spectral point for both illumination directions we have $A_p = A_m = A_M = A > A_Q$, it is clearly seen from Fig. 7b,d. The spectral changes of the phases calculated for the multipole terms are shown in Fig. 9. For the illumination from top (Fig. 9a) the phases of all multipole terms are near zero at $\lambda = 674$ nm, so one can approximate them, as $\varphi_p = \varphi_Q = \varphi_M \approx 0$ and $\varphi_m \neq 0$, and write

$$r \approx i|C|(A_Q - Ae^{i\varphi_m}), \tag{25}$$

$$t \approx 1 + i|C|(Ae^{i\varphi_m} - A_Q). \tag{26}$$

For the illumination from cones' base (Fig. 9b) the phases behavior is different at $\lambda = 674$ nm comparing with the above case. However, again all phases are close to zero but $\varphi_p = \varphi_Q \neq 0$ and $\varphi_m \approx \varphi_M \approx 0$, so one can estimate

$$r \approx i|C|([A + A_Q]e^{i\varphi_p} - 2A), \tag{27}$$

$$t \approx 1 + i|C|(A - A_Q)e^{i\varphi_p}. \tag{28}$$

Because of in the both cases the phases are small, the reflection suppression is corresponded to the small value of $(A - A_Q)$ that could be considered as a generalized Kerker condition.

For the both illumination schemes there are also two spectral points with the almost zero transmission at the wavelengths $\lambda = 707$ nm and $\lambda = 794$ nm (Fig. 7a,d). These effects are provided by the resonant excitation of TED ($\lambda = 707$ nm) and MD moments ($\lambda = 794$ nm). Small disagreements between the spectral positions of the dipole resonances and the transmission zeros observed in Fig.7, are explained by the weak contributions of other multipoles. Interestingly, the phase difference between the TED and MD terms in the electric field reflection and transmission coefficients is the same and equals to $\pi/2$ for the both illumination schemes at $\lambda = 707$ nm and $\lambda = 794$ nm (Fig. 9). As a result one can estimate the reflection coefficient as

$$|r|^2 \sim |(iA_p - A_m)|^2 = A_p^2 + A_m^2. \tag{29}$$

In the proximity to the TED and MD resonances, the interaction between them provides maximum reflection and minimum transmission.

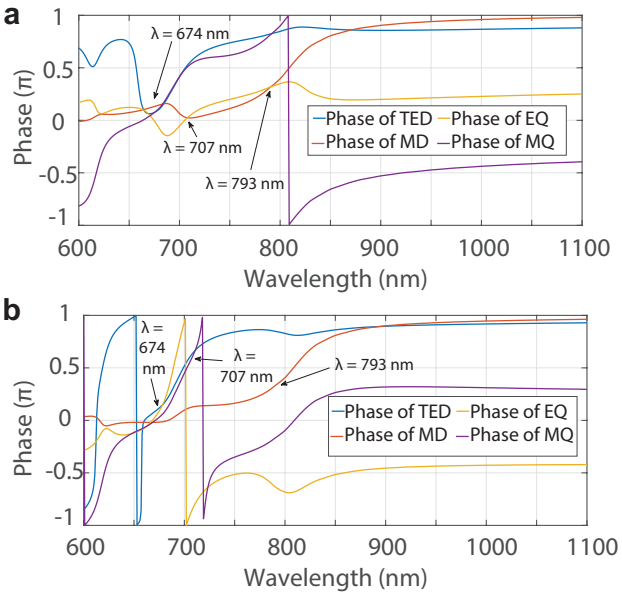

Figure 9: Phases of the multipole terms in the electric field reflection and transmission coefficients r and t of the metasurface composed of nanocones ($H = 300$ nm, $D_c = 300$ nm) with the period $D = 450$ nm. (a) Illumination from the apex side of the nanocones, (b) illumination from the base edge of the nanocones. The definition of the phase is explained in the main text.

IV. CONCLUSION

In this work we have presented the technique that allows to make a multipole analysis of the transmission and reflection spectra of metasurfaces composed of periodically arranged nanoparticles. We have revealed how the analytical multipole decompositions of field reflection and transmission coefficients of nanoparticle arrays can be obtained from the single particle scattering. It has also been demonstrated that the multipole analysis allows to explain the origins of the reflection and transmission features. The developed approach has been applied for the multipole analysis of the reflection and transmission properties of the metasurfaces (2D arrays) composed of silicon nanocubes or nanocones. In the case of the nanocubes, the "lattice invisibility (anapole) effect" has been found and discussed. It has been shown that this effect corresponds to the light transmission through a metasurface almost without amplitude and phase perturbations, however, with the excitation of basic multipole moments. For the metasurfaces composed of conical nanoparticles illuminated from different sides, it has been shown that the transmission does not depend on the illumination schemes whereas the reflection and absorption can be different, because of different electric field distributions inside the nanoparticles for the same wavelength.

We have demonstrated that our method is applicable to the arrays composed of arbitrarily shaped nanoparticles. In this case, full-wave numerical calculations need to be applied. The multipole analysis explaining the observed reflective and transmitting properties of the array and can be applied for tuning its geometrical parameters to achieve required functionality of the metasurface.

Thus, for the application aspects of our approach, two main positions can be pointed out. The first advantage is a direct application of our technique. In this case, the developed method can be used both for investigations of the influence of inter-particle interactions inside arrays on the multipole optical response of nanoparticles and for a theoretical explanation of spectral transmission and reflection features of the arrays. After investigations of the multipole response in the arrays, this information can be used for optimization of the array optical properties. For instance, the optimization can be done by tuning overlaps of different multipole resonances those spectral positions are determined by the particle's geometry and array periods. Multipole decompositions of the array fields and analysis of transmission and reflection spectra give us more precise and effective tool for theoretical optimization of nanoparticle arrays. The second advantage is the possibility to use multipole response of single nanopar-

ticles for the estimation of the optical properties of the arrays composed of them. Using our method we showed how the array surrounding affects and changes the multipole response of nanoparticles. Frequently, the array surrounding only slightly disturbs the spectral distribution of multipole resonances of single dielectric nanoparticles. It means we can use spectral multipole behavior of single nanoparticles for the qualitative design of nanoparticles arrays with given optical properties.

Acknowledgments

A.B.E. thanks Alexey Krasavin and Margoth Cordova Castro for useful and productive discussions. This work has been supported by the Israeli Ministry of Trade and Labor-Kamin Program, Grant. No. 62045. A.S.S acknowledges the support of the Russian Fund for Basic Research within the projects 18-02-00414, 18-52-00005 and the support of the Ministry of Education and Science of the Russian Federation (GOSZADANIE Grant No. 3.4982.2017/6.7). The development of analytical approach and the calculations of multipole moments have been supported by the Russian Science Foundation Grant No. 16-12-10287. Support has been provided by the Government of the Russian Federation (Grant No. 074-U01). The research described was performed as a part of the joint Ph.D. program between the BGU and ITMO. V.E.B. work is supported by the Air Force Office of Scientific Research under Grant No. FA9550-16-1-0088.

Appendix: Expressions for the multipole moments

For the Cartesian multipole moments following expressions have been used:

$$\mathbf{p} = \int \mathbf{p} j_0(kr) d\mathbf{r} + \frac{k^2}{10} \int \left\{ [\mathbf{r}\cdot\mathbf{P}]\mathbf{r} - \frac{1}{3} r^2 \mathbf{P} \right\} \frac{15 j_2(kr)}{(kr)^2} d\mathbf{r},$$

$$\mathbf{m} = -\frac{i\omega}{2} \int [\mathbf{r}\times\mathbf{P}] \frac{3 j_1(kr)}{kr} d\mathbf{r},$$

$$\hat{Q} = \int \left\{ 3(\mathbf{r}\otimes\mathbf{P} + \mathbf{P}\otimes\mathbf{r}) - 2[\mathbf{r}\cdot\mathbf{P}]\hat{U} \right\} \frac{3 j_1(kr)}{kr} d\mathbf{r} + 6k^2 \int \{ 5\mathbf{r}\otimes\mathbf{r}[\mathbf{r}\cdot\mathbf{P}] - (\mathbf{r}\otimes\mathbf{P} + \mathbf{P}\otimes\mathbf{r}) r^2 - r^2 [\mathbf{r}\cdot\mathbf{P}]\hat{U} \right\} \frac{j_3(kr)}{(kr)^3} d\mathbf{r},$$

$$\hat{M} = \frac{\omega}{3i} \int \{ [\mathbf{r}\times\mathbf{P}]\otimes\mathbf{r} + \mathbf{r}\otimes[\mathbf{r}\times\mathbf{P}] \} \frac{15 j_2(kr)}{(kr)^2} d\mathbf{r},$$

where $\mathbf{p}$, $\mathbf{m}$, $\hat{Q}$, $\hat{M}$ are the multipole moments in the Cartesian representation, and j_n denotes n-order spherical Bessel function, k is the wavenumber in air. All expressions based on light-induced polarization $\mathbf{P}(\mathbf{r}) = \varepsilon_0(\varepsilon_{Si} - 1)\mathbf{E}(\mathbf{r})$, where ε_0 and ε_{Si} are the vacuum permittivity and relative dielectric permittivity of silicon. $\mathbf{E}(\mathbf{r})$ is the total electric field inside the nanoparticle. We also use the electric octupole moment expressions from Ref.[17,54].

* Electronic address: terekhovpd@gmail.com
† Electronic address: alinak@bgu.ac.il
‡ Electronic address: a.b.evlyukhin@daad-alumni.de

[1] A. B. Evlyukhin, C. Reinhardt, A. Seidel, B. S. Lukyanchuk, and B. N. Chichkov, Physical Review B **82**, 045404 (2010).
[2] A. I. Kuznetsov, A. E. Miroshnichenko, M. L. Brongersma, Y. S. Kivshar, and B. Lukyanchuk, Science **354**, aag2472 (2016).
[3] S. Jahani and Z. Jacob, Nature Nanotechnology **11**, 23 (2016).
[4] I. Staude and J. Schilling, Nature Photonics **11**, 274 (2017).
[5] A. Krasnok, M. Caldarola, N. Bonod, and A. Alú, Advanced Optical Materials **6**, 1701094 (2018).
[6] A. B. Evlyukhin, S. M. Novikov, U. Zywietz, R. L. Eriksen, C. Reinhardt, S. I. Bozhevolnyi, and B. N. Chichkov, Nano Letters **12**, 3749 (2012).
[7] A. I. Kuznetsov, A. E. Miroshnichenko, Y. H. Fu, J. Zhang, and B. Lukyanchuk, Scientific reports **2**, 492 (2012).
[8] A. A. Basharin, M. Kafesaki, E. N. Economou, C. M. Soukoulis, V. A. Fedotov, V. Savinov, and N. I. Zheludev, Physical Review X **5**, 011036 (2015).
[9] A. B. Evlyukhin, C. Reinhardt, and B. N. Chichkov, Physical Review B **84**, 235429 (2011).
[10] P. K. Jain, X. Huang, I. H. El-Sayed, and M. A. El-Sayed, Plasmonics **2**, 107 (2007).
[11] M. I. Stockman, Optics express **19**, 22029 (2011).
[12] A. Karabchevsky, A. Mosayyebi, and A. V. Kavokin, Light: Science & Applications **5**, e16164 (2016).
[13] J. B. Khurgin, Nature Nanotechnology **10**, 2 (2015).
[14] A. E. Krasnok, A. E. Miroshnichenko, P. A. Belov, and Y. S. Kivshar, Optics Express **20**, 20599 (2012).
[15] B. Rolly, B. Stout, and N. Bonod, Optics Express **20**, 20376 (2012).
[16] P. D. Terekhov, K. V. Baryshnikova, A. S. Shalin, A. Karabchevsky, and A. B. Evlyukhin, Optics Letters **42**, 835 (2017).
[17] P. D. Terekhov, K. V. Baryshnikova, Y. A. Artemyev, A. Karabchevsky, A. S. Shalin, and A. B. Evlyukhin, Phys-

ical Review B **96**, 035443 (2017).
[18] T. Shibanuma, T. Matsui, T. Roschuk, J. Wojcik, P. Mascher, P. Albella, and S. A. Maier, ACS Photonics **4**, 489 (2017).
[19] M. R. Shcherbakov, D. N. Neshev, B. Hopkins, A. S. Shorokhov, I. Staude, E. V. Melik-Gaykazyan, M. Decker, A. A. Ezhov, A. E. Miroshnichenko, I. Brener, et al., Nano Letters **14**, 6488 (2014).
[20] G. Grinblat, Y. Li, M. P. Nielsen, R. F. Oulton, and S. A. Maier, Nano Letters **16**, 4635 (2016).
[21] A. S. Shorokhov, E. V. Melik-Gaykazyan, D. A. Smirnova, B. Hopkins, K. E. Chong, D.-Y. Choi, M. R. Shcherbakov, A. E. Miroshnichenko, D. N. Neshev, A. A. Fedyanin, et al., Nano Letters **16**, 4857 (2016).
[22] D. G. Baranov, S. V. Makarov, V. A. Milichko, S. I. Kudryashov, A. E. Krasnok, and P. A. Belov, ACS Photonics **3**, 1546 (2016).
[23] J.-F. Li, Y.-J. Zhang, S.-Y. Ding, R. Panneerselvam, and Z.-Q. Tian, Chemical Reviews **117**, 5002 (2017).
[24] D. G. Baranov, R. Verre, P. Karpinski, and M. Käll, ACS Photonics (2018).
[25] O. Yavas, M. Svedendahl, P. Dobosz, V. Sanz, and R. Quidant, Nano Letters **17**, 4421 (2017).
[26] P. Terekhov, K. Baryshnikova, A. Evlyukhin, and A. Shalin, Journal of Physics: Conference Series **929**, 012065 (2017).
[27] S. M. Kamali, E. Arbabi, A. Arbabi, and A. Faraon, Nanophotonics (2018).
[28] D. Lin, P. Fan, E. Hasman, and M. L. Brongersma, Science **345**, 298 (2014).
[29] J. Cheng, D. Ansari-Oghol-Beig, and H. Mosallaei, Optics Letters **39**, 6285 (2014).
[30] I. Staude, A. E. Miroshnichenko, M. Decker, N. T. Fofang, S. Liu, E. Gonzales, J. Dominguez, T. S. Luk, D. N. Neshev, I. Brener, et al., ACS Nano **7**, 7824 (2013).
[31] M. Decker, I. Staude, M. Falkner, J. Dominguez, D. N. Neshev, I. Brener, T. Pertsch, and Y. S. Kivshar, Advanced Optical Materials **3**, 813 (2015).
[32] A. Arbabi, Y. Horie, M. Bagheri, and A. Faraon, Nature Nanotechnology **10**, 937 (2015).
[33] V. E. Babicheva and A. B. Evlyukhin, Laser & Photonics Reviews **11** (2017).
[34] M. Kerker, D.-S. Wang, and C. Giles, JOSA **73**, 765 (1983).
[35] Y. Nagasaki, M. Suzuki, and J. Takahara, Nano Letters **17**, 7500 (2017).
[36] T. Wood, M. Naffouti, J. Berthelot, T. David, J.-B. Claude, L. Métayer, A. Delobbe, L. Favre, A. Ronda, I. Berbezier, et al., ACS Photonics **4**, 873 (2017).
[37] M. I. Shalaev, J. Sun, A. Tsukernik, A. Pandey, K. Nikolskiy, and N. M. Litchinitser, Nano Letters **15**, 6261 (2015).
[38] P. Spinelli, M. Verschuuren, and A. Polman, Nature Communications **3**, 692 (2012).
[39] V. Raghunathan, D. Borlaug, R. R. Rice, and B. Jalali, Optics Express **15**, 14355 (2007).
[40] J. S. T. Gongora, A. E. Miroshnichenko, Y. S. Kivshar, and A. Fratalocchi, Nature Communications **8**, 15535 (2017).
[41] N. Odebo Lank, R. Verre, P. Johansson, and M. Kall, Nano Letters **17**, 3054 (2017).
[42] C.-Y. Yang, J.-H. Yang, Z.-Y. Yang, Z.-X. Zhou, M.-G. Sun, V. E. Babicheva, and K.-P. Chen, ACS Photonics (2018).
[43] C. F. Bohren and D. R. Huffman, Absorption and scattering of light by small particles (John Wiley & Sons, 2008).
[44] J. D. Jackson, Classical electrodynamics (Wiley, 1999).
[45] R. Alaee, C. Rockstuhl, and I. Fernandez-Corbaton, Optics Communications **407**, 17 (2018).
[46] Y. Yang, A. E. Miroshnichenko, S. V. Kostinski, M. Odit, P. Kapitanova, M. Qiu, and Y. S. Kivshar, Physical Review B **95**, 165426 (2017).
[47] V. E. Babicheva and A. B. Evlyukhin, ACS Photonics **5**, 2022 (2018).
[48] V. Kravets, A. Kabashin, W. Barnes, and A. Grigorenko, Chemical Reviews (2018).
[49] V. Savinov, V. A. Fedotov, and N. I. Zheludev, Physical Review B **89**, 205112 (2014).
[50] E. Shahmoon, D. S. Wild, M. D. Lukin, and S. F. Yelin, Physical Review Letters **118**, 113601 (2017).
[51] A. E. Miroshnichenko, A. B. Evlyukhin, Y. F. Yu, R. M. Bakker, A. Chipouline, A. I. Kuznetsov, B. Luk'yanchuk, B. N. Chichkov, and Y. S. Kivshar, Nature Communications **6**, 8069 (2015).
[52] A. A. Basharin, V. Chuguevsky, N. Volsky, M. Kafesaki, and E. N. Economou, Physical Review B **95**, 035104 (2017).
[53] R. Fleury, F. Monticone, and A. Alù, Physical Review Applied **4**, 037001 (2015).
[54] A. B. Evlyukhin, T. Fischer, C. Reinhardt, and B. N. Chichkov, Physical Review B **94**, 205434 (2016), URL `http://link.aps.org/doi/10.1103/PhysRevB.94.205434`.
[55] R. E. Raab and O. L. De Lange, Multipole theory in electromagnetism: classical, quantum, and symmetry aspects, with applications, vol. 128 (Oxford University Press on Demand, 2005).
[56] L. D. Landau and E. M. Lifshitz, The classical theory of fields (Pergamon, 1971).
[57] A. B. Evlyukhin, C. Reinhardt, E. Evlyukhin, and B. N. Chichkov, JOSA B **30**, 2589 (2013).